Atmospheric Research 305 (2024) 107447

Contents lists available at ScienceDirect

Atmospheric Research

journal homepage: www.elsevier.com/locate/atmosres

# Benefits of the coupling in the downscaling the South American climate

Jorge Ordoñez [a], Jonathan Paredes [a], Rubén Vázquez [b,*], Alan Llacza [a], Gerardo Jacome [a], Gustavo De la Cruz [a], Jorge Llamocca [a], Delia Acuña [a], Dmitry V. Sein [c,d], Erick Álvarez [e], William Cabos [b]

[a] Sub-Directorate of Numerical Modeling of the Atmosphere, National Service of Meteorology and Hydrology, Lima, Peru
[b] Departamento de Física y Matemáticas, Universidad de Alcalá, Alcalá de Henares, Madrid, Spain
[c] Department of Climate Dynamics, Alfred Wegener Institute for Polar and Marine Research, Bremerhaven, Germany
[d] Shirshov Institute of Oceanology, Russian Academy of Science, Moscow, Russia
[e] La Molina National Agrarian University, Lima, Peru

ARTICLE INFO

*Keywords:*
Regional coupled model
Climate simulations
Humboldt upwelling system
El Niño 1 + 2 region

ABSTRACT

We evaluate the benefits of the use of a regional coupled model over its stand-alone atmospheric component when forced by reanalysis data in the simulation of the South American climate. We find that the coupling allows for a better simulation of important features of the atmospheric circulation and surface temperature. The simulated 2 meters air temperature is improved over most of the continent, the sea level pressure over the South Pacific Anticyclone area is better represented in the coupled simulation and the location of the ITCZ is improved during the austral winter. The precipitation, especially over the Andes, benefits less from the coupling, although a more realistic humidity transport leads to a reduction of the precipitation biases over extensive regions. The austral summer precipitation bias is reduced in areas such as eastern Colombia, northern Bolivia, eastern Brazil and central Argentina. For austral winter, the coupled model has a better performance in a large part of the Amazon region, in areas such as east of Peru, west Brazil, north Bolivia and south Argentina. Moreover, the regionally coupled model not only improves the simulation of important features of the observed atmospheric fields but also demonstrates good skills in reproducing the Humboldt upwelling system. Therefore, our study highlights the advantages of regional coupled models for the simulation of the South American climate, as the ocean-atmosphere interaction is of utmost importance for the circulation mechanisms that determine the climate of the region.

## 1. Introduction

The climate of South America is shaped by its complex orography, dominated by the presence of the Andes Mountains and the Amazonian plains and the influence of the surrounding oceans (e.g., Espinoza et al., 2020). Besides, it is influenced by ocean-land-atmosphere interactions and large-scale oceanic and atmospheric circulation patterns. Among them, the displacements and changes in strength of South Atlantic Convergence Zone, the South Atlantic Anticyclone (SAA), the South Pacific Anticyclone (SPA) and the Intertropical Convergence Zone (ITCZ) play an important role. For instance, the poleward branch of the SPA influences the meridional winds along the coastal zone of Chile and Peru, contributing to the formation of the Humboldt current upwelling system (one of the most important fishery grounds at the world; Pauly and Christensen, 1995) and to the existence of the desertic coastal region that stretches from southern Equator down to central Chile (Rahn and Garreaud, 2014). Furthermore, the seasonal north-south migration of the ITCZ in the northern parts of South America and the eastern branch of the SAA (which brings humid Tropical Atlantic air masses to the Amazonian region) trigger latitudinal and seasonal variations in the South America climate (Drumond et al., 2014).

Along with the large scale, regional variations of the temperature and precipitation are influenced by the semipermanent Chaco Low (CL), the Bolivian High (BH), and the South American low-level jet (e.g., Espinoza et al., 2020; Segura et al., 2019). Additionally, the strengthening of the Upper-Level Jet has been observed during El Niño events, which favors storm and convective conditions (Bruick, 2019). At interannual and decadal time scales, the climate variability is strongly

* Corresponding author.
*E-mail address:* ruben.vazquezm@uah.es (R. Vázquez).

https://doi.org/10.1016/j.atmosres.2024.107447
Received 13 December 2023; Received in revised form 5 March 2024; Accepted 26 April 2024
Available online 27 April 2024

determined by the El Niño Southern Oscillation (ENSO) and the Pacific Decadal oscillation. (e. g. Garreaud et al., 2009; Cai et al., 2020). The effects of these climate models in different regions are modulated by other large-scale climate patterns as the Antarctic Oscillation (Silvestri and Vera, 2003).

Therefore, there is a need for an accurate representation of the climate in the region, both for process and impact studies. Climate models, both global and regional, are very important tools for this task, especially for understanding the future evolution of climate under different scenarios. In particular, atmosphere-ocean regionally coupled models (Sein et al., 2015; Lewis et al., 2018; Cabos et al., 2019; Xue et al., 2020; Bielli et al., 2021; Thompson et al., 2021) make possible simulations of the climate system at higher resolution than global climate models, improving our understanding of the finer features of climate variability, and extreme events. Moreover, being forced by reanalysis data, they are better constrained to observations than global models in simulations of present time climate while being able to adequately represent ocean-atmosphere feedbacks inside the model domain (Sein et al., 2015).

Many studies have shown the ability of regional atmospheric models in reproducing the current South American climate (Silvestri et al., 2009; Carril et al., 2012). However, few studies have explored the impact of the representation of ocean-atmosphere interaction processes on the simulation of the South American and Eastern Pacific climate using high resolution atmosphere-ocean regionally coupled models (Pezzi et al., 2023; Xie et al., 2007; Ambrizzi et al., 2019). In order to fill this gap, we introduce a new setup of ROM, a widely used ocean-atmosphere regionally coupled model in order to evaluate the possible benefits that coupling brings in the representation of the South American and eastern Pacific climate. For this evaluation we analyze the performance of the coupled model and its stand–alone atmospheric component in simulating the main large-scale systems that characterize the climate in the area of study, as well as the response of the coupled regional climate system to ENSO variability and the patterns of rainfall and temperature over the region.

To date, most of the downscaling of global simulations is done using an atmospheric regional model coupled to a land surface scheme and driven over ocean by prescribed sea surface temperature (SST). However, there are regions where the atmosphere-ocean feedback can substantially influence the spatial and temporal structure of regional climate (Li et al., 2012). Recent studies have shown that Regional Climate System Models (RCSMs) are capable of simulating features of the climate system that otherwise are not resolved by state-of-the-art global climate models due to their low resolution or by the atmospheric only regional model due to the lack of the representation of the ocean-atmospheric coupling and/or the low resolution of the SST used to force them (Soares et al., 2019; Parras-Berrocal et al., 2020; de la Vara et al., 2021). Therefore, compared to GCMs, RCSMs can achieve much higher resolution and detailed parameterizations, providing a more accurate representation of the relevant small-scale processes (Sein et al., 2020) and compared to RCMs, the interaction between the ocean and atmosphere in RCMSs also give a more realistic representation of the physic mechanisms than in atmosphere and ocean only regional models (Sein et al., 2015).

In Section 2 and 3 we present the model configurations, in Section 4 the results and discussion are presented and finally the summary and conclusions are presented in Section 5.

## 2. The ROM coupled system

ROM is a coupled system comprising the REgional atmosphere MOdel (REMO; Jacob and Podzun, 1997), the oceanic model of the Max Planck Institute (MPIOM; Marsland et al., 2003; Jungclaus et al., 2006), the Hamburg oceanic carbon cycle model (HAMOCC; Marsland et al., 2003), the hydrological discharge model (HD; Hagemann and Dumenil-Gates, 1998, 2001) and a dynamic/thermodynamic sea ice model (Hibler, 1979). REMO and MPIOM are coupled through the OASIS3 coupler (Valcke, 2013), while HAMOCC and HD are run as modules of MPIOM and REMO respectively. ROM has been applied to climate studies in different areas, demonstrating the benefits of regional coupling (e.g Cabos et al., 2020; Parras-Berrocal et al., 2020; Vázquez et al., 2022; Vázquez et al., 2023). For instance, ROM has also been applied to the simulation of the Central American climate (Cabos et al., 2019), demonstrating a good representation of the ocean and atmosphere circulation.

### 2.1. The atmospheric component

REMO is a three-dimensional hydrostatic atmospheric model formulated in a hybrid system of sigma-pressure coordinates in the vertical direction and in a rotated grid with Arakawa C discretization in the horizontal. The physical parameterizations in the version of REMO used in this work come from ECHAM model versions 4 and 5 (Sein et al., 2015, Table 1).

### 2.2. The oceanic component

The Max Planck Institute Oceanic Model (MPIOM) was developed in Germany (Jungclaus et al., 2013). In the horizontal, it uses curvilinear orthogonal coordinates on an Arakawa C grid. The vertical discretization in the z coordinate (Sein et al., 2015). The MPIOM horizontal resolution can be refined near the mesh poles, allowing for a high resolution in the region of interest while maintaining a global domain. In ROM, MPIOM uses a global grid, allowing trapped coastal waves (originating from outside the coupled domain) to influence the variability of the barotropic sea level and the bottom pressure in the coupled domain.

### 2.3. Coupling strategy

The atmospheric and oceanic components are coupled with a time step of 3 h with the OASIS3 coupler, while the hydrological discharge model HD interchanges information with REMO and MPIOM with a frequency of 24 h (Fig. 1a). In the coupled region MPIOM receives heat, freshwater and momentum fluxes from REMO and in turn provides the sea surface conditions to REMO. For the rest of the global ocean, MPIOM calculates the heat, freshwater and momentum flows from the global model used for boundary conditions with a bulk formulation. HD receives surface runoff and drainage from REMO and delivers river and freshwater fluxes to MPIOM (Sein et al., 2015). Both the atmospheric lateral boundary conditions and the atmospheric forcing for the ocean outside the area of coupling are obtained from global reanalysis and GCMs simulations. In the last case, the propagation of the biases in the global model into the interior of the region of coupling can be compensated, as the regional model simulates its own climate, largely

**Table 1**
Description of the parameterization in the REMO and MPIOM.

| | Parameterization | Reference |
|---|---|---|
| Regional atmospheric model (REMO) | Longwave radiation | Fouquart and Bonnel (1980) |
| | Shortwave radiation | Mlawer et al. (1997) |
| | Cumulus | Tiedtke (1989) and Nordeng (1994) |
| | Microphysics | Lohmann and Roeckner (1996) |
| Global Ocean Model (MPIOM) | Bottom boundary layer slope | Marsland et al. (2003) |
| | Harmonic horizontal diffusion | Griffies (1998) |
| | Eddy-induced tracer transport | Gent et al. (1995) |
| | Deep convection | Marsland et al. (2003) |

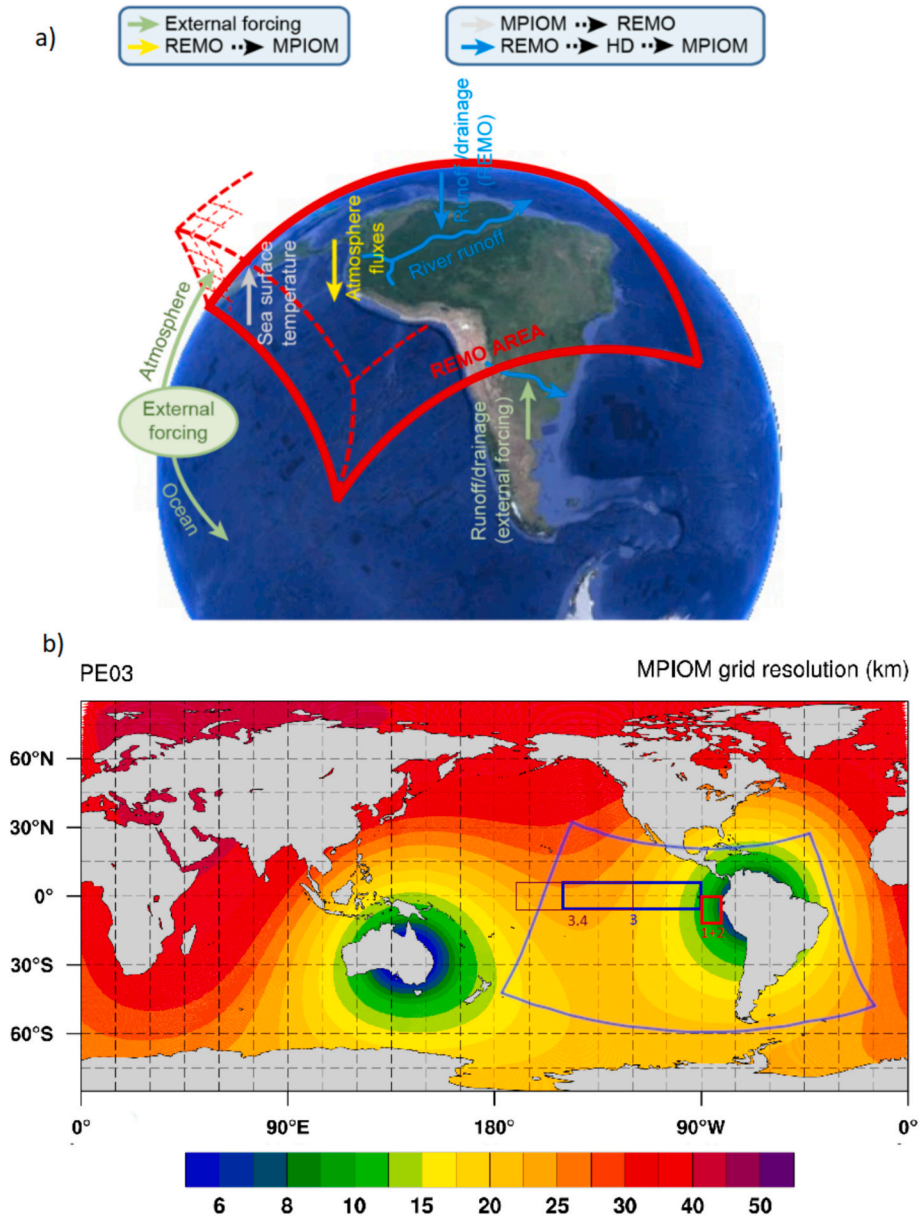


**Fig. 1.** a) Coupling scheme for ROM. The atmosphere and the ocean are coupled in the region covered by the REMO domain. The MPIOM and HD domains are global. b) Spatial domain of the MPIOM (shaded) and REMO (thick line over South America).

independent of the global model (Sein et al., 2015). Some parameters for the atmospheric and oceanic components of ROM are presented in Table 1.

## 3. Numerical simulations

The coupled and uncoupled climate simulations used in this study share the same REMO configuration. In the coupled simulations, REMO is run in a rotated mesh of constant resolution and the global MPIOM has its higher resolution in the area of coupling (which matches the REMO domain; Sein et al., 2015). The REMO domain has a spatial resolution of 24 km and extends from 60°S to 30°N and from 175°W to 14°W (Fig. 1b), extending the South America–CORDEX (Coordinated Regional Climate Downscaling Experiment Project) domain. This enlarged South America–CORDEX domain includes the parts of the Atlantic and Pacific Oceans that directly influence the climate of South America (Garreaud et al., 2009). In particular, it covers El Niño 1 + 2 (defined as the box bounded by 10°S, 0°, 90°W, 80°W), Niño 3 (5°N–5°S, 150°W–90°W), and part of El Niño 3.4 (5°N-5°S, 120°-170°W) regions. As stated above, the REMO domain determines the region of coupling in ROM and the MPIOM rotated poles are placed in the north of South America and in Western Australia (Fig. 1b). This configuration provides a finer grid ~8 km near the eastern coast of South America and 24 km in the central Pacific. The simulations cover the years 1980–2017, a period in which strong ENSO events occurred (Sulca et al., 2018).

### 3.1. Experimental design

For present time, two simulations were carried out with the ERA-Interim reanalysis as the initial and boundary conditions. The scheme in Fig. 2 summarizes the two simulations performed, as well as our spin-up strategy. The spin-up period for REMO and ROM were 2 and 130 years respectively. The ROM spin up was carried out in 3 phases: in the first phase MPIOM was run for 50 years (1958–2002) forced by ERA 40. In the second phase, starting from the final state of the MPIOM run, a coupled simulation was carried out for the 1980–2017 period, also

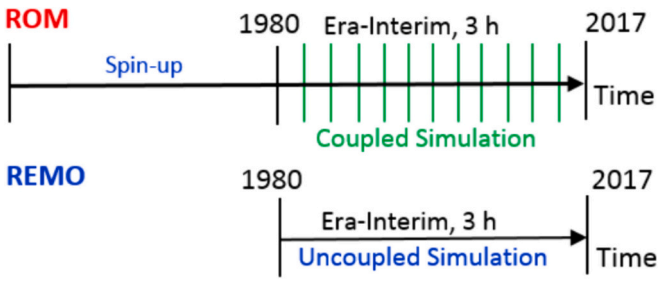


**Fig. 2.** Schematic of the modeling systems used in the study: coupled (ROM) and uncoupled (REMO) simulations.

forced by ERA-Interim. In the third phase, a new coupled simulation forced by ERA 40 was performed for the period 1958–2001, starting from the final state of the previous simulation. We resorted to this simulation as a significant warming trend in SST in the run forced by ERA-Interim was observed. This made problematic the use of the final state of that simulation as the initial state of the production run. After the last ERA-40 forced run, a quasi-equilibrium state in better concordance with the oceanic observed state at the beginning of 1980 was reached. Therefore, the final state of this run was used as initial conditions for the production simulation. Table 2 shows some details of the simulations, such as the spatial resolutions and the vertical levels.

## 4. Assessment strategy

The model outputs were assessed and compared in terms of seasonal cycle and inter-annual variability. For the validation, we use monthly data of the most representative atmosphere and ocean variables: near-surface air temperature (T2m), sea surface temperature (SST), wind, precipitation, sea level pressure (SLP), specific humidity in 200 hPa and 850 hPa and ocean temperature. Taken together, these variables allow for the evaluation of the models' ability to represent climate at both large and local scales.

In order to carry out this validation, various statistics were performed with the aim of quantitatively demonstrating the improvement of coupling compared to stand-alone models. To evaluate the performance of the ROM and REMO against ERA5 reanalysis, were calculated the Root Mean Squared Error (RMSE) and Pearson correlation coefficient (r), defined as follows:

$$RMSE = \sqrt{\frac{1}{n}\sum_{i=1}^{n} REF_i - MODEL_i}$$

where REFi denotes the measured parameter obtained from ERA5 and MODELi the corresponding parameter obtained from the ROM and REMO model. Pearson correlation coefficient is defined as follows:

**Table 2**
Summary of the characteristics of the two simulations.

| Simulation | Forcing/ period | Coupler OASIS3 | MPIOM spatial resolution (km) | REMO spatial resolution (km) | Number of hybrid levels |
|---|---|---|---|---|---|
| REMO | ERA-Interim/ 1980–2017 | Not coupled | – | 24 | 31 |
| ROM | ERA-Interim/ 1980–2017 | Coupled | 8–24 | 24 | 31 |
| ROM spin-up | ERA-Interim/ 1980–2017 | Coupled | 8–24 | 24 | 31 |
| ROM spin-up | ERA-40/ 1958–2001 | Coupled | 8–24 | 24 | 31 |

$$r_{REF,MODEL} = \frac{cov(REF, MODEL)}{\sigma_{REF}\sigma_{MODEL}}$$

We calculate probability density functions (PDFs). From PDFs, we calculate the cumulative minimum value of two distributions, thereby measuring the common area between two PDFs. If a model simulates the observed conditions perfectly, the Perkin score (PS) will equal one, which is the total sum of the probability at each bin center in a given PDF (Perkins et al., 2007):

$$PS = \sum_{bin=1}^{bin=N} min\left(PDF_{MODEL,} PDF_{REF}\right)$$

Finally, in order to measure the added value of the regional atmosphere–ocean coupling on simulated precipitation using CHIRPS, TERRA and ERA5, we apply the formula of Weber et al. (2023) as follows:

$$AV = \frac{(REMO - REF)^2 - (ROM - REF)^2}{MAX\left[(REMO - REF)^2, (ROM - REF)^2\right]}$$

where AV is the added value, REMO and ROM are the simulated precipitation and T2m of the models, and REF are the respective reference data sets.

## 5. Results and discussion

### 5.1. Wind field and humidity

The most remarkable regional feature of the atmospheric circulation over South America at the upper levels is the BH (Lenters and Cook, 1997; Espinoza et al., 2020), which is found at 200 hPa in DJF (Fig. 3a; contour lines). The BH core position, located around 15°S and 65°W in ERA5 (Hersbach et al., 2020) is well represented in REMO and ROM, although both simulations present a slight southeast displacement. The BH position enhances the occurrence of convective clouds which contribute to the distribution and the magnitude of the accumulated precipitation in the Andes and Amazon area of Peru. Thus, the highest values of specific humidity (HUS, shading in Fig. 3) are found in the Amazon above 30°S. The REMO and ROM experiments underestimate the specific humidity (Fig. 3a) with biases that reach 0.03 g/kg in the region of higher HUS values. Also on the eastern coast of Brazil, the high-level anticyclonic circulation associated with BH (Virji, 1981; Chen et al., 1999; Espinoza et al., 2020) leads to a lower specific humidity above this region. Similar results can be found for the two models in JJA, when the specific humidity is underestimated in regions north of the equator, demonstrating the ability of both simulations to reproduce the seasonal and spatial structure of the summer circulation (Silvestri et al., 2009; Reboita et al., 2022).

Near the surface, the large-scale circulation is dominated by the ITCZ, the SPA and the SAA. The SAA in the simulation domain is strongly influenced by ERA-Interim, as it is mostly outside of the domain. The two models simulate well the large-scale surface circulation (Fig. 3c-d) in the two seasons. In DJF, REMO is closer to ERA5 in the region of the ITCZ (Fig. 3 c), where ROM overestimates slightly the HUS. Nevertheless, both models simulate the ITCZ position in a similar way (Fig. S1). Also, both REMO and ROM show higher values of the HUS (above 13 g/kg at 850 hPa) on the eastern slopes of the Andes and the Amazon. However, in the austral winter (JJA), the coupling leads to a better representation of the HUS (Fig. 3 d) and the surface circulation (Fig. S2).

It is noteworthy a lower HUS over the Humboldt upwelling system in DJF, especially in ROM. This signal may be associated with the upwelling periods, since the coastal surface waters present temperatures that are lower than those of the atmosphere, therefore, the air adjacent to the sea surface cools and its relative humidity increases. Note that the differences found between ROM and REMO are significant for the entire domain in both seasons (Fig. S3c and f; Fig. S4c and f).

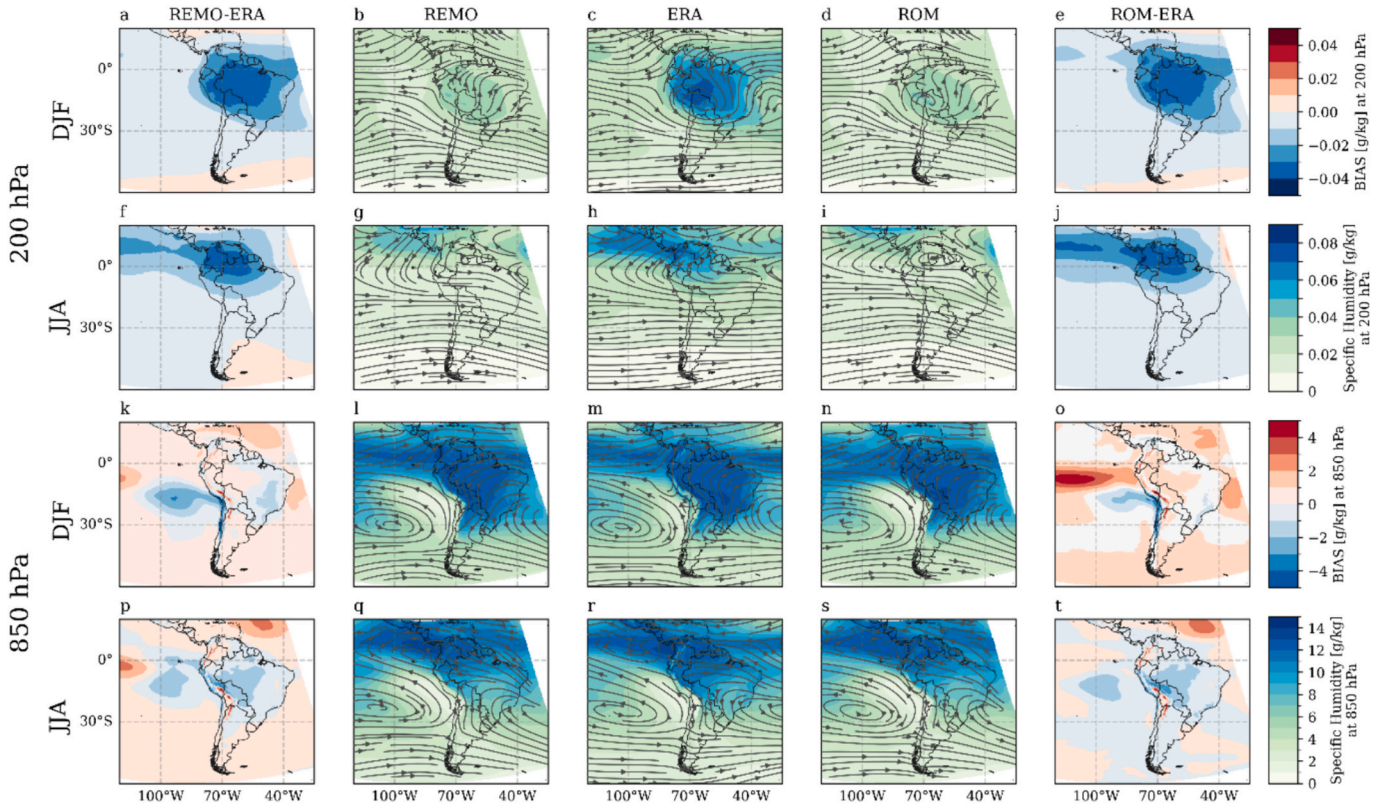


**Fig. 3.** a) and b) Climatology of specific humidity and current lines at 200 hPa for 1982–2011. c) and d) Climatology of specific humidity and current lines at 850 hPa for 1982–2011. The first and last columns show the distribution of the biases of REMO-ERA5 and ROM-ERA5, respectively.

### 5.2. Sea level pressure

The surface large-scale circulation in the South American Pacific sector is dominated by the semi-permanent SPA, which is located off the coast of Chile (see Fig. 4) When the SPA is further north, precipitation over Chile is higher, while it is lower in the east of Argentina, much of Brazil, Peru, Bolivia and Ecuador (Barrett and Hameed, 2017). In DJF, ROM reproduces the southern SPA migration better than REMO, and simulates SLP intensities closer to ERA5 (around 1020 hPa; Fig. 4, upper panels).

In the austral summer, the location of the SPA core starts to shift north until passes the 30°S parallel in the austral winter (JJA; Fig. 4, lower panels), determining conditions of the predominance of stratiform cloudiness on the coasts of Peru (Schemenauer et al., 1988). In this season, the ERA5 pressure in the SPA is near 1018 hPa, which is well reproduced by ROM (Fig. 4j) and underestimated by REMO (2 hPa; Fig. 4f). So, in both seasons, ROM represents better than REMO (with significant differences; Fig. S5f) the core of the ERA5 SPA, both in location and intensity, demonstrating the benefits of an interactive ocean for the simulation of the characteristic patterns of the circulation in the atmospheric lower levels.

In order to assess the impact of coupling on the representation of the

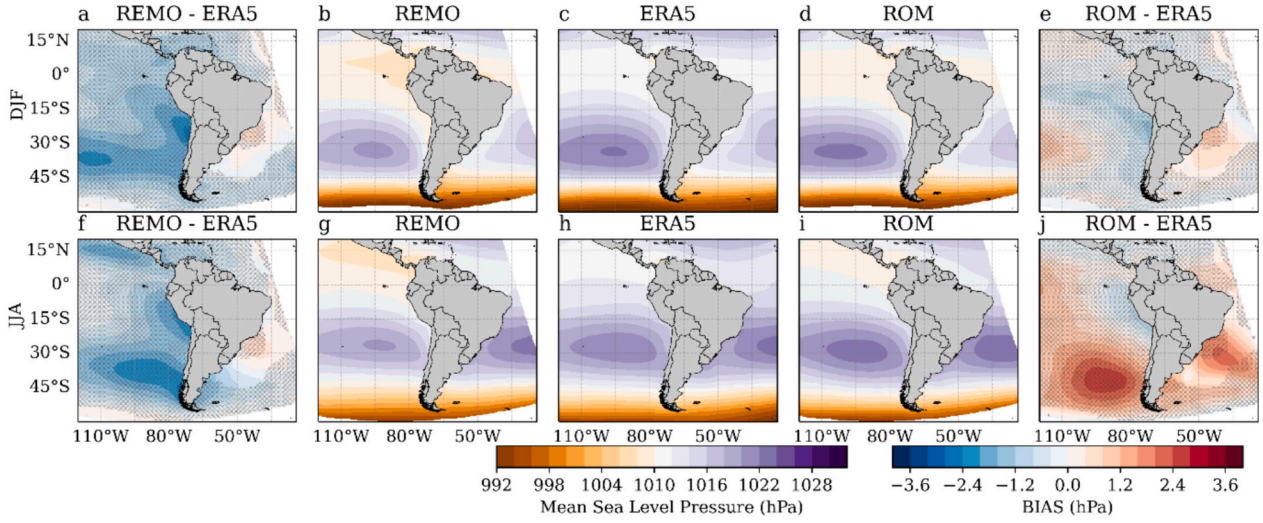


**Fig. 4.** SLP Climatology for 1982–2011. The first and last columns show the distribution of the biases of REMO-ERA5 and ROM-ERA5, respectively. Black dots present the regions where the differences are significant.

temporal evolution (seasonal and interannual variability), we analyze the SLP averaged over the Niño 1 + 2 and SPA region.

The SLP annual cycle in El Niño 1 + 2 (Fig. 5a) reaches values around 1013 hPa in August–September and 1011 hPa in March. In general, there is a clear improvement of the seasonal cycle in the coupled simulation. Moreover, ROM simulates better the Probability Density Function (PDF) than REMO, being closer to ERA5 for both seasons (Fig. 6. b and 6. c). This improvement is reflected by the Perkins scores: 0.50 and 0.41 for ROM and REMO respectively in DJF and 0.70 for ROM, 0.50 for REMO in JJA.

On the other hand, REMO shows a better representation of the interannual variability of the SLP over the Niño1 + 2 region in DJF (Fig. 5d), although the correlations are non-significant for both simulations. In JJA both simulations present a better representation of the SLP (Fig. 5e), showing significant correlations with ERA5 (0.56 and 0.59 for REMO and ROM respectively). It is worth noting that the Niño1 + 2 SLP anomalies in REMO and ROM show a general agreement with ERA5 except during the extraordinary El Niño events 1982–83 and 1997–98, when ROM does not simulate well the strong SLP drops that characterize those events. This fact is related to the prescribed ERA-Interim SST in REMO, which improves the drop in SLP during these events.

In the SPA region, we use the box defined by the coordinates [10° S - 50° S] and [130° W - 70° W] (Ancapichún and Garcés-Vargas, 2015). Here, the seasonal cycle is also better represented in ROM (Fig. 6.a), showing an overestimation from May to November. This improvement leads to a better representation of the surface wind along the Pacific and the coastal regions in both seasons (Fig. S2). The improvement is also reflected in the PDF (Fig. 6 b and c), with ROM showing consistently higher Perkin scores than REMO in both seasons: 0.92 (ROM), 0.84 (REMO) in DJF and 0.93 (ROM), 0.84 (REMO) in JJA. Furthermore, the interannual variability (Fig. 6. d and e), measured by the standard deviation, in the SPA is similar in both simulations, 0.64 and 0.62 for REMO and ROM respectively in DJF and 0.84 and 0.81 for REMO and ROM respectively in JJA.

### 5.3. Air temperature

In DJF, the ERA5 T2m shows the highest values over land in the North SA–Central America and northeast Brazil and the lowest values in the Andes and the southernmost part of the continent (Fig. 7). Although the spatial distribution of the biases over land is similar in both models, the magnitude is lower in ROM (specially in northeastern Brazil and Chaco plains, Fig. 7). This could be related to a better simulation of the South American monsoon system (Vuille et al., 2012). ROM also shows lower biases over the dry Pacific coastal regions. Over the ocean, biases in ROM present a more complex pattern than in REMO, which only presents positive biases. The coupling leads to negative biases near the Pacific coasts, south of the equator and in the subtropics, with positive biases in the tropical interior oceans. Those biases reach its higher value in front of the Peru northern coast and the southern Ecuador coasts, in the Niño 1 + 2 region.

In JJA, the T2m biases in both simulations are generally lower than in DJF over the continent. ROM is closer to ERA5 than REMO, showing weaker positive biases. Over the ocean, REMO presents a quite uniform bias distribution in the range of 0 to 1 °C, associated with the SST forcing (ERA-Interim). The ROM biases range between −1.6 °C off Chile coast (related to the representation of the upwelling processes) and 4 °C in the region of confluence of the Malvinas and Brazil currents. Noteworthy, the coupled simulation bias becomes stronger in the Niño 1 + 2 region, where the overestimation reaches values close to 4 °C. The results obtained at both seasons are opposite to those obtained by Falco et al. (2019), who found cold biases in most RCMs and GCMs across practically the entire South American continent.

To quantify the improvements in the representation of T2m over land due to the coupling, the added value (AV) was calculated following Eq. 4. Positive AV values indicate that the regional climate model (ROM) T2m is closer to ERA5 than REMO. For DJF (Fig. 8a), positive AV values are observed over most of the continent, except for some coastal regions. During JJA (Fig. 8b), positive AV values persist, except for eastern Brazil and the Peruvian coast.

### 5.4. Precipitation

The precipitation of the coupled and uncoupled model were compared against ERA5, CHIRPS (Funk et al., 2015) and TerraClimate (Abatzoglou et al., 2018). In DJF, REMO and ROM biases show the largest differences in the eastern slope of the Andes in Peru, Bolivia, Ecuador and Colombia (Fig. 9). In these regions, both simulations overestimate the precipitation (around 850 mm/season) in all comparisons (less in ERA5), which could be related to a stronger orographic

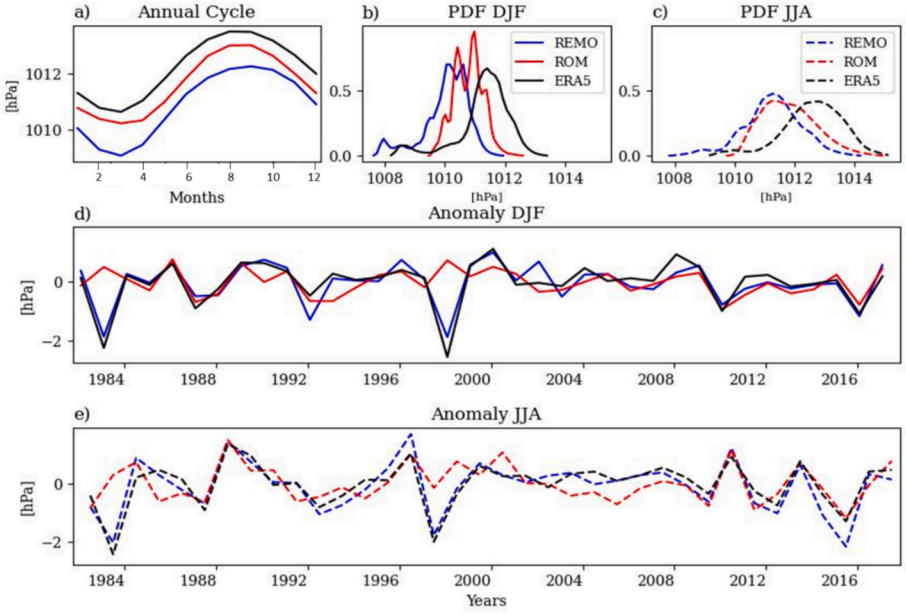


**Fig. 5.** SLP over El Niño 1 + 2 region. a) Annual cycle for ERA5, REMO, and ROM. Probability Density Function for b) DJF and c) JJA. Seasonal anomalies for d) DJF and e) JJA.

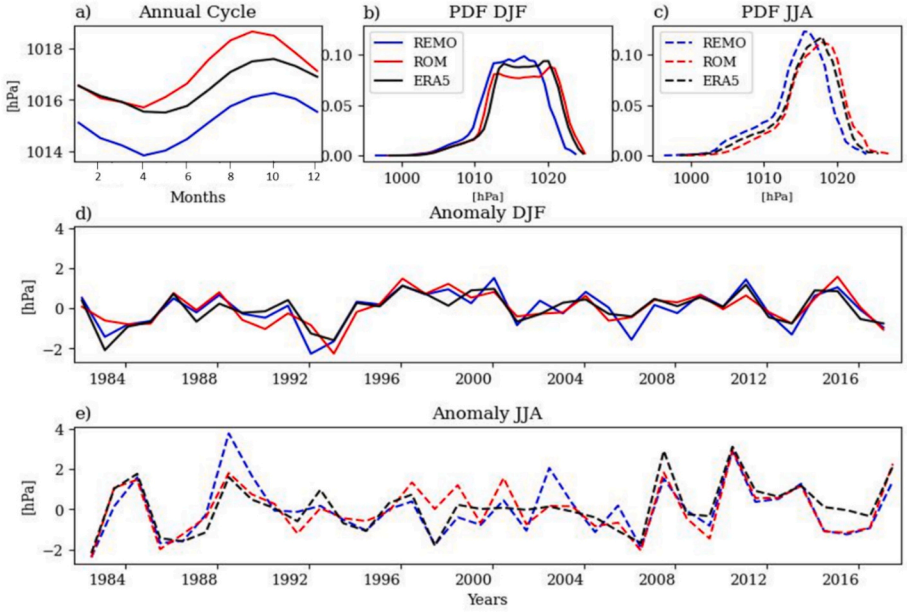


**Fig. 6.** SLP over (SPA) region. a) Annual cycle for ERA5, REMO, and ROM. Probability Density Function for b) DJF and c) JJA. Seasonal anomalies for d) DJF and e) JJA.

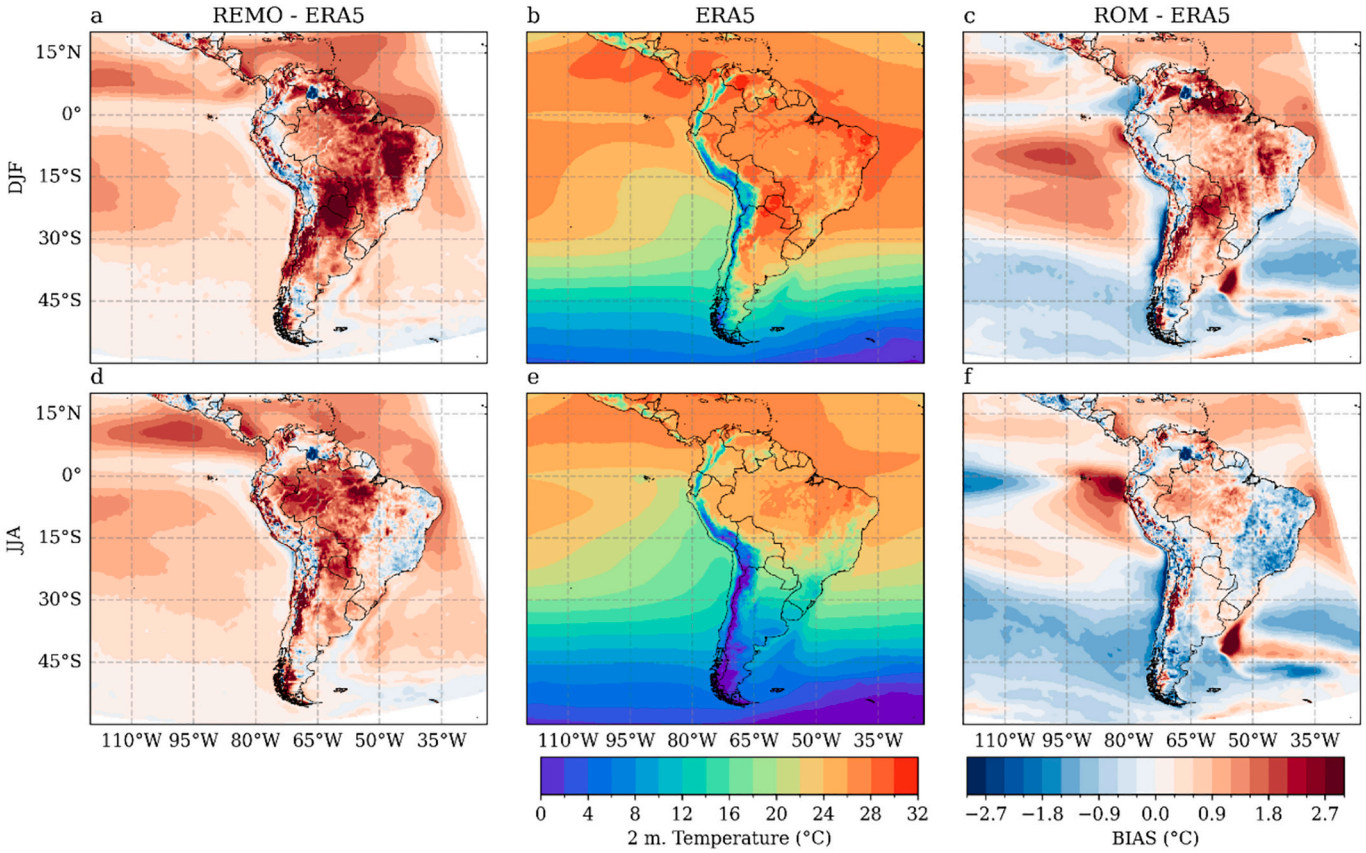


**Fig. 7.** Distribution and spatial comparison of the 1982–2011 climatology simulation of the T2m for DJF (summer) and JJA (winter). The first and last columns show the distribution of biases REMO-ERA5 and ROM-ERA5, respectively.

convective precipitation in the models (Giorgi et al., 2016), which was also found by Llopart et al. (2020) using an ensemble of GCMs and another one from the South America CORDEX. Negative biases (smaller in magnitude than the positive) are also found, especially in the north-eastern regions of SA, the forest areas of central, southern Peru and northern Bolivia. It is noteworthy that these biases cover smaller areas in ROM than in REMO, showing also lower values.

For JJA, the positive biases over the north and central Andes are reduced in the two models. Both models underestimate the precipitation in the northeast of the continent, with biases ranging from −640 to

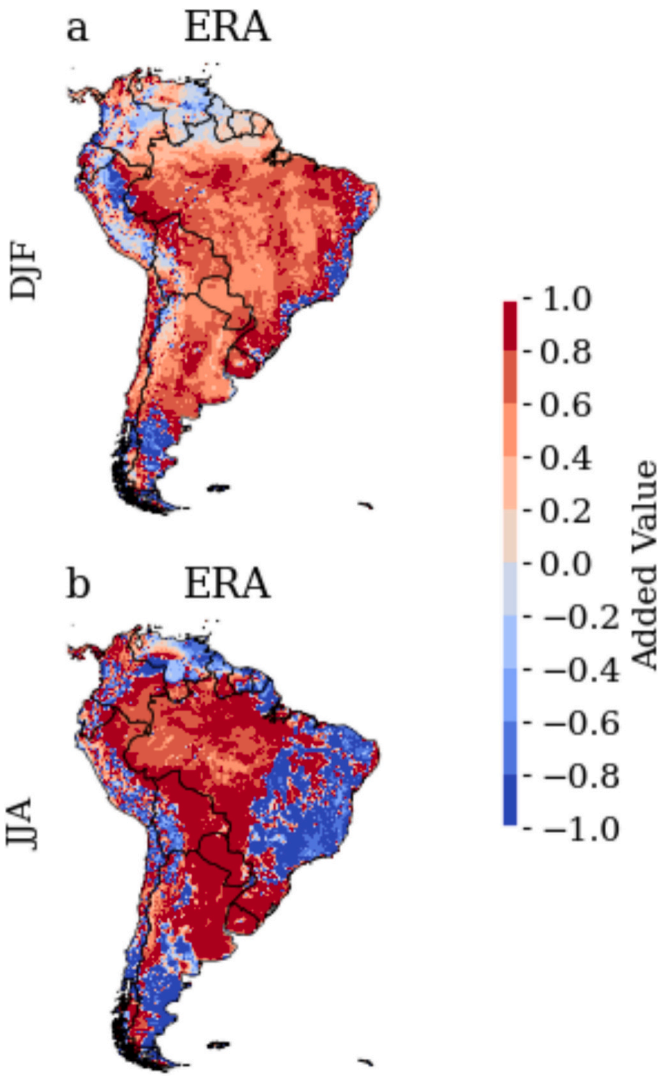


**Fig. 8.** Added value AV of seasonal mean T2m for entire South America in ROM compared to REMO. Reference data set is ERA5, for (a) December to February (DJF) and (b) July to August (JJA). Positive (negative) values indicate a lower (higher) precipitation bias of ROM compared to REMO.

−240 mm/season. Positive biases with respect to the three datasets are found in western Colombia and the eastern part of the central Andes in Peru, reaching values from 350 to750 mm/season. However, only when ROM is compared with TERRA and CHIRPS the positive biases extend to the western part of the Ecuadorian territory. Sánchez et al. (2015) found that precipitation is mostly underestimated, especially over South America, by climate models (both GCMs and RCMs). However, here we show that this underestimation does not occur in all regions, primarily along the western coast of South America.

The improvements of the simulated precipitation by the coupling is reflected by the AV (Fig. 10). In DJF, ROM improves the precipitation mainly in zones as east of Brazil,Colombia and central Argentina. In JJA, the coupled model performs better than uncoupled over east of the Andes mountains range, west Brazil, north Bolivia and south Argentina. This fact is comparable to the improvement shown by the RCMs over the GCMs in Llopart et al. (2020), where in this case the coupling plays a greater added value compared to the RCMs.

In the El Niño 1 + 2 region, ROM and REMO overestimate the annual cycle, being the overestimation more evident in ROM for austral summer (Fig. 11a). In the PDF it is notable how the coupling influences the representation of the precipitation in DJF, where ROM is not able to reproduce the maximum frequency distribution (Fig. 11b). For JJA the frequency distributions are similar in both models, detecting the maximum frequency as ERA5 (Fig. 11c). Nevertheless, ROM is able to reproduce the march of the ERA5 seasonal cycle. The amplitude of the interannual variability is well reproduced by ROM and REMO, although REMO presents higher correlations with ERA5 in both seasons (ROM with 0.58 and 0.40, and REMO, 0.68 and 0.76 in DJF and JJA respectively). Both models underestimate the magnitude of the precipitation anomalies, especially during the strong 1982–1983 and 1997–1998 El Niño events (Fig. 11 d y e). The fact that REMO better reproduces the Niño 1 + 2 index from ERA5 than ROM is primarily associated with REMO being surface-forced by ERA-Interim, resulting in a closer approximation to the observations. In this case, ROM overestimates the SST of ERA5 in the Niño 1 + 2 region (see the following section), leading to increased evaporation and consequently an overestimation of precipitation.

### 5.5. Sea surface temperature

The OSTIA (Stark et al., 2007) SST, along with ROM and REMO biases are shown in Fig. 12 for DJF and JJA. The eastern Pacific SST shows two very characteristic features: the equatorial cold tongue, a region where temperatures drop to about 24 °C (Penven et al., 2005) and a pool of warm waters with SST above 26 °C, located between 5°N and 10°N and associated with the latitudinal shifts of the ITCZ (Kang et al., 2020). These spatial characteristics are present in ROM in both seasons and, in general, the magnitude of their biases in the eastern Pacific is usually <2 °C. Positive biases are observed off the northern coast. However negative biases are found for other regions as off the coast of Chile. In DJF, these biases are stronger in the warm pool and are associated with biases in the simulation of the ITCZ in this season (Fig. 12c). In JJA although the ITCZ is better represented by ROM, a cold bias is reflected in the cold tongue (Fig. 12f), which is related to the underestimation of precipitation (Fig. S2 and Fig. S7). This fact was found in Zou and Zhou (2011) over the western North Pacific simulated by a regional ocean-atmosphere coupled model. The persistent warm anomalies in the coastal regions of the cold tongue can be related to a lack of upwelling due to too weak meridional coastal winds off Peru (Vannière et al., 2014) or to a too deep mixed layer, which could prevent the upwelling of colder deeper water, effectively reducing the associated cooling. A cold coastal bias that extends from the south of Chile up to 19°S during DJF, signaling a stronger upwelling. The bias has less intensity north of 14°S and reverses signs in JJA (Fig. 12f).

The warm biases in the eastern part of the cold tongue (Fig. 12c and f) are reflected in the seasonal cycle of the Niño 1 + 2 index (Fig. 13a). There, ROM SST follows the seasonal march of the OSTIA SST, although displaces the seasonal maximum from March to April and is warmer for most of the year. The warm biases also influence the PDFs: the ROM PDF is displaced to the right of OSTIA by about 2 °C in the two seasons (Fig. 13 b and c). In DJF, the mode of the distribution for ROM is located between 25 and 26 °C while in OSTIA it is between 24 and 25 °C. In JJA the SST is again overestimated, with the higher frequency between 25 and 26 °C in ROM and 23–24 °C in OSTIA. Finally, we validate the interannual SST variability, characterized by the root mean square error (RMSE). Although ROM reproduces well the interannual SST variability, it is not able to simulate the amplitude of the stronger ENSOs, underestimating the intensity of the 1982–1983 and 1997–1998 Niño. The RMSE values found for ROM are (1.3 for DJF and 1.5 for JJA) and for REMO (0.24 for DJF and 0.33 for JJA).

The equatorial ocean-atmospheric variability near the coast can be represented by the Coastal El Niño Index (ENCI, Fig. 14), defined as the 3-months running mean of the monthly SST anomalies averaged over the El Niño 1 + 2 (Takahashi et al., 2014). The Coastal El Niño Index time series for the 1981–2017 period is represented in Fig. 14 for ERA5, REMO (i.e. ERA-Interim) and ROM. Generally, ROM reproduces the ENCI variability, although during the strongest events it significantly

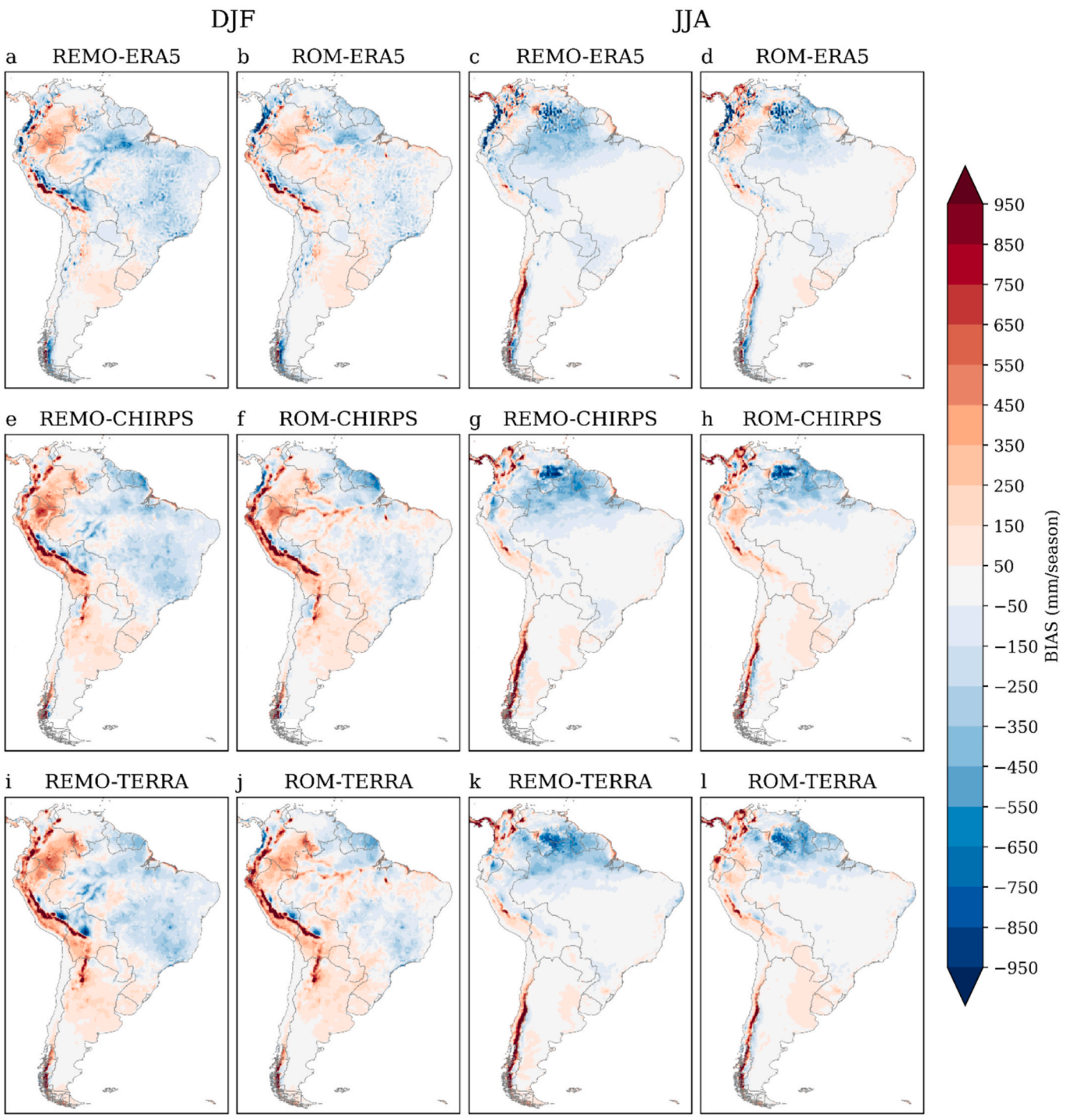


**Fig. 9.** Spatial distribution of the average annual precipitation in 1982–2011 for DJF (summer) and JJA (winter), simulated by ROM and REMO.

underestimates the ERA5 ENCI values. The RMSE values obtained for ROM were (0.62 for DJF and 1.04 for JJA) and with the SST from ERA-Interim used to REMO was (0.15 for DJF and 0.22 for JJA).

### 5.6. *Upwelling coastal temperature*

One of the main advantages of the regional coupled simulations is the possibility to evaluate the ocean variables with a higher resolution than the state of the art climate and reanalysis models. In this case, the model domain includes one of the most important ecosystems in the world, the Humboldt upwelling region, which is part of the eastern boundary current that flows along the south American Pacific coasts (García-Reyes et al., 2015). In this section, we assess the ability of ROM to reproduce the signal of the upwelling. For this, we show the cross-shore section in 15°S and 30°S for DJF(Fig. 15) and JJA (Fig. 16). We compare our results with SODA reanalysis (Carton et al., 2018) and IMARPE (Marine Institute of Peru) datasets (Domíngues et al., 2017).

In DJF, IMARPE data shows an offshore stratified thermal structure for both 15°S and 30°S. The 16 °C isotherm in the coastal regions upwells from around 120 m in 15°S and almost from 200 m in the case of 30°S. ROM represents this feature well in both temperature and depth, with apparently no differences with SODA. It is noteworthy that ROM

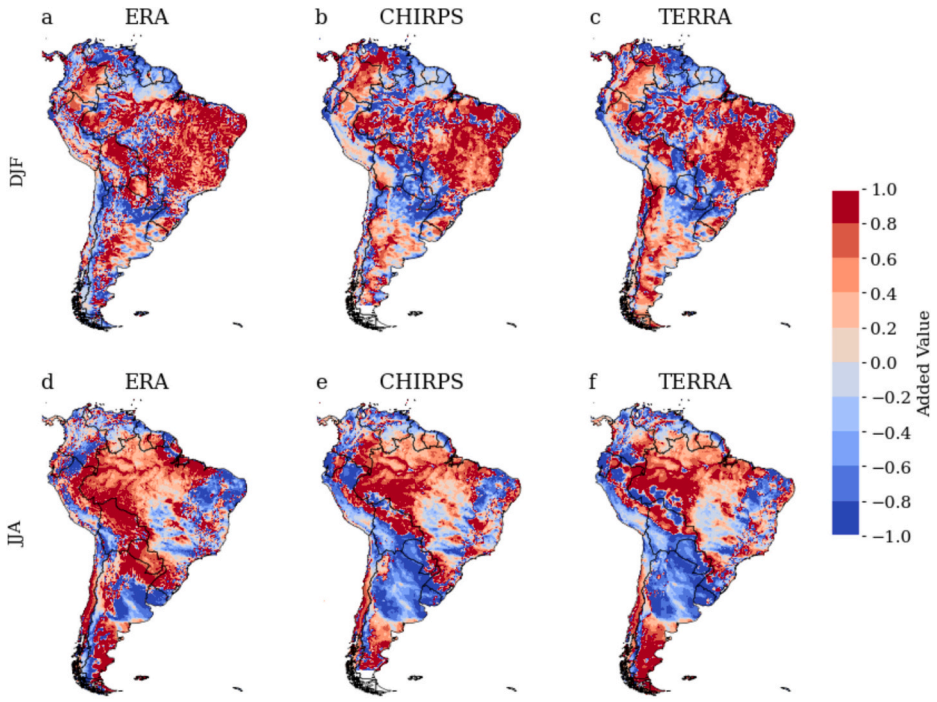


**Fig. 10.** Precipitation Added value over SA of ROM compared to REMO. Reference data sets are ERA5, CHIRPS and TERRA. Positive (negative) values indicate a lower (higher) precipitation bias of ROM compared to REMO.

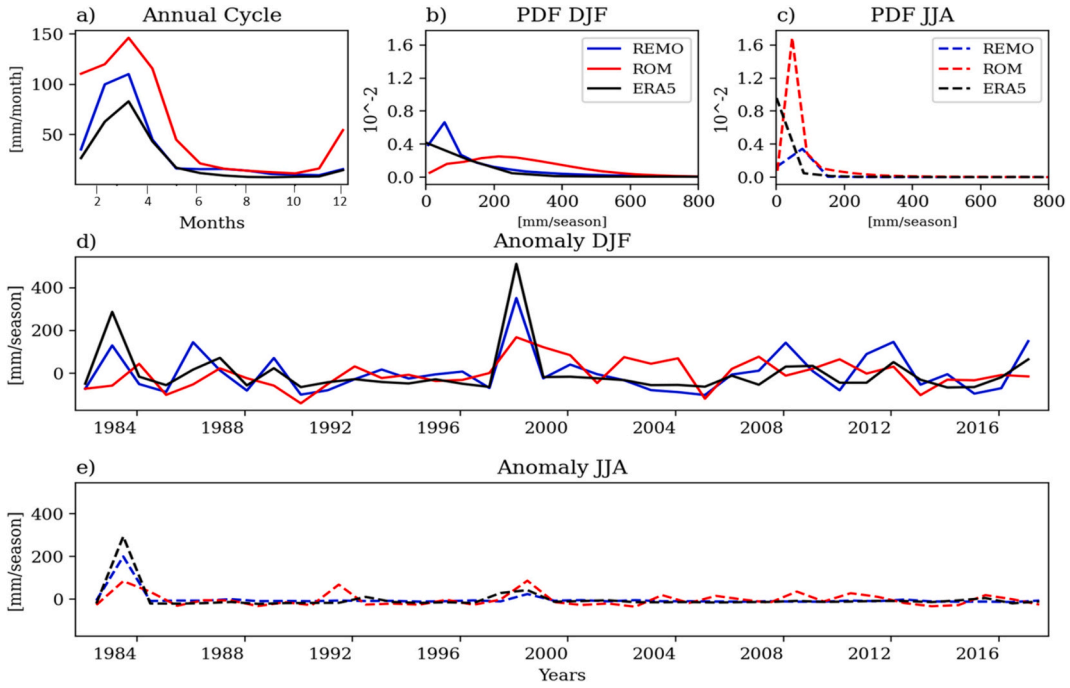


**Fig. 11.** Precipitation over El Niño 1 + 2 region. a) Annual cycle for ERA5, REMO, and ROM. Probability Density Function for b) DJF and c) JJA. Seasonal anomalies for d) DJF and e) JJA.

accurately reproduces the temperature vertical structure between 100 and 200 m near the coast better than SODA, probably due to a higher resolution here (e.g. Vázquez et al., 2022). Also ROM reproduces better the deepening of the upwelling at 30°S, providing a good latitudinal representation of the Humboldt upwelling system (e.g. Oyarzún and Brierley, 2019).

Since the Humboldt upwelling is practically non-seasonal from 5°S to 40°S (Kämpf and Chapman, 2016), the two cross-sectional transect in JJA presents a structure very similar to that in DJF. In both latitudes, ROM reproduces well the thermal vertical structure of the upwelling. However, SODA seems to overestimate the upwelling at 30°S, leading to clearly colder temperatures at the surface for regions closer to the coast. Therefore, ROM is able to reproduce better than SODA the observed latitudinal and seasonal structure of the Humboldt upwelling system.

The ROM's ability to reproduce coastal upwelling opens the possibility of assessing with great accuracy the impact of climate change on

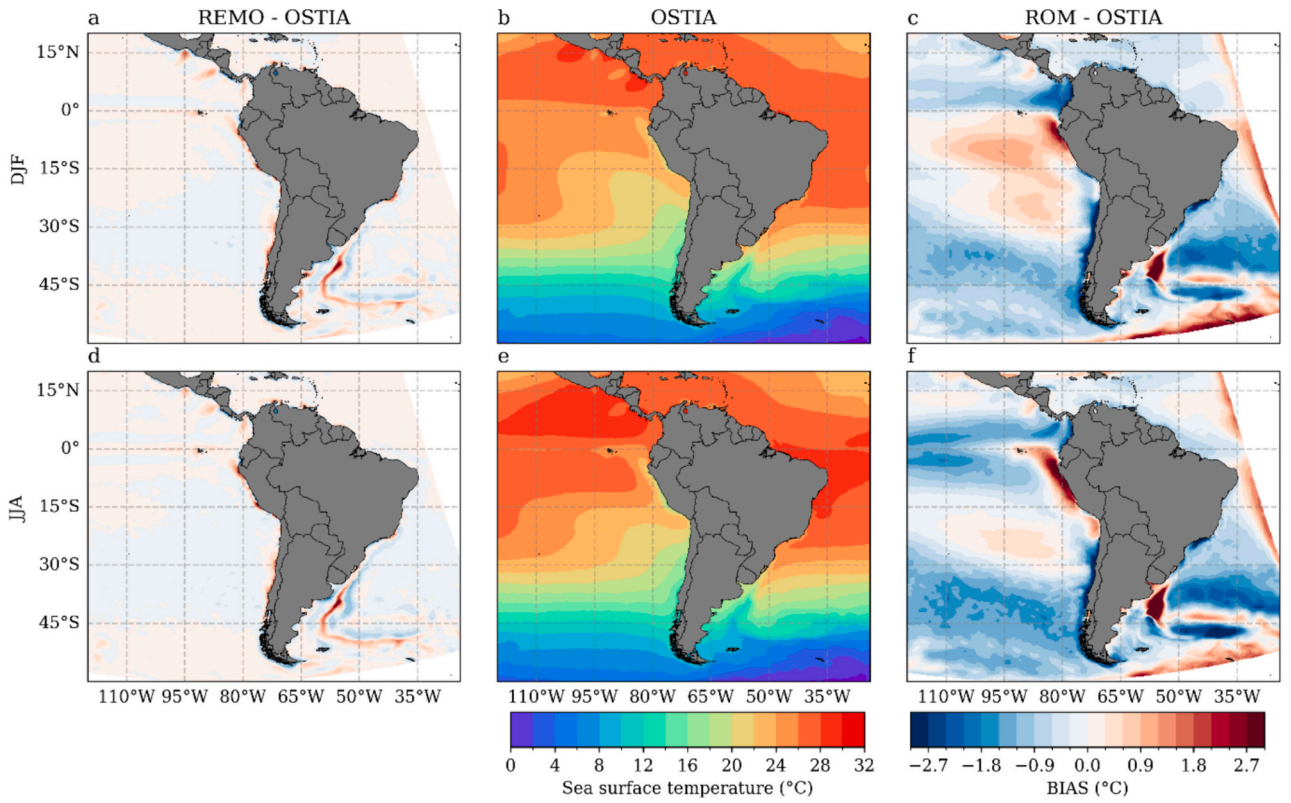


**Fig. 12.** Climatology of the sea surface temperature (SST) for 1982–2011. The distribution of the REMO-OSTIA and ROM-OSTIA bias for the DJF summer and JJA winter, respectively, is shown.

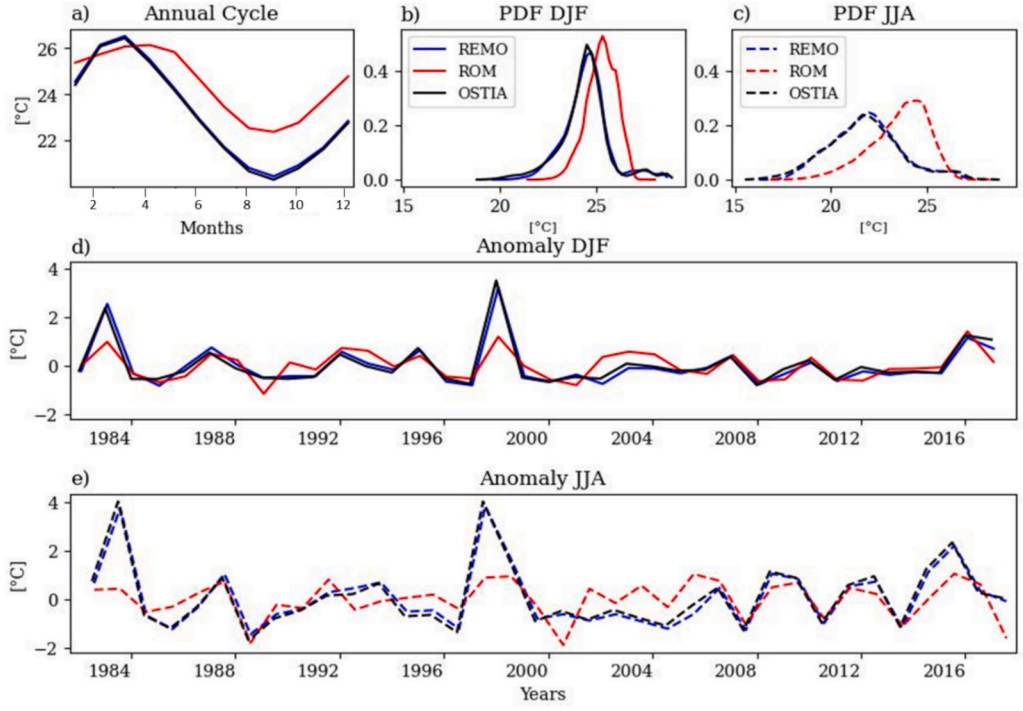


**Fig. 13.** SST over El Niño 1 + 2 region. a) Annual cycle for ERA5, REMO, and ROM. Probability Density Function for b) DJF and c) JJA. Seasonal anomalies for d) DJF and e) JJA.

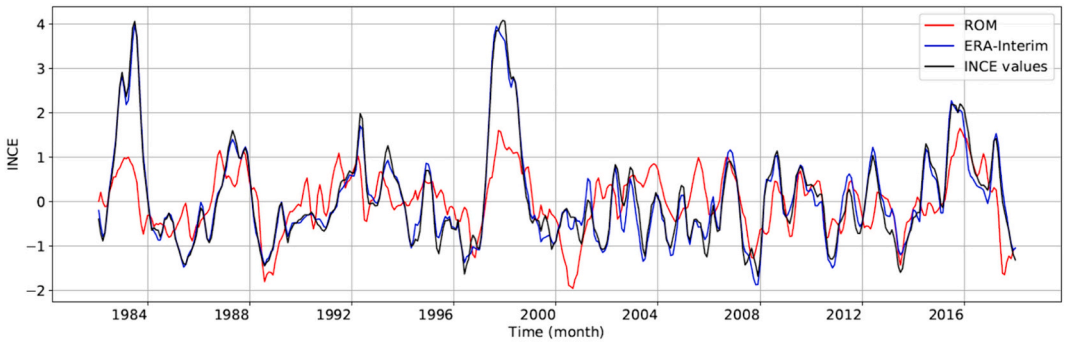


**Fig. 14.** El Niño Coastal Index (ENCI) for ROM, REMO (ERA-Interim) and ENCI values (Source http://met.igp.gob.pe/datos/icen.txt).

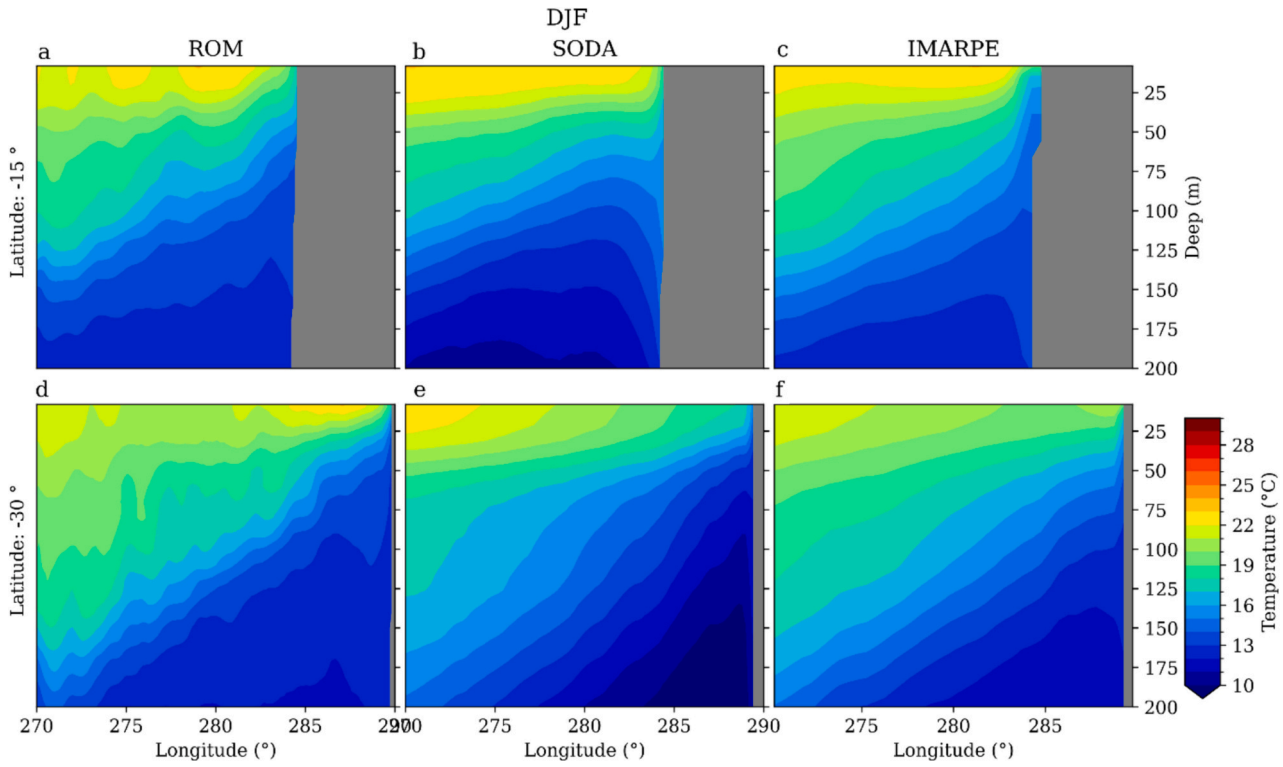


**Fig. 15.** Cross-shore temperature (°C) transect for DJF in 15°S (upper) and 30°S (lower) for ROM, SODA and IMARPE in DJF.

the coastal upwelling, as well as the mechanisms responsible for them.

## 6. Conclusions

A detailed assessment of the regional climate, both present and future, requires increasingly sophisticated tools. State of the art GCMs are able to capture the large-scale mechanisms, while RCMs, which downscale the GCM climate variables, provide higher horizontal resolution in specific regions. However, as these RCMs only represent the atmosphere or ocean independently, important processes, influenced by ocean-atmospheric interactions can be missed in the downscaled signal. Therefore, in this study, we propose to assess the ability of the atmosphere-ocean regionally coupled model, ROM (REMO-OASIS-MPIOM) to simulate the climate of the South American continent and the surrounding ocean, and compare it with its atmospheric component REMO, which prescribes the ERA-Interim SST.

In order to simulate the climate of the South American continent and the relevant ocean-atmosphere interactions, our simulation covers a large domain that includes the eastern tropical Pacific and most of the Niño3 region. Therefore, it is important to assess the ability of our coupled model to accurately reproduce the most important large-scale mechanisms. For instance, both REMO and ROM reproduce well the upper-level high-pressure centers (Bolivian high), reproducing well the associated atmospheric circulation and humidity distribution. This is not unexpected, as at the upper atmospheric levels, the influence of the coupling should not be important. However, the impact of the coupling is clearly seen in the simulation of the ITCZ, as it is heavily influenced by the location of the region of high SST, which is prescribed in the REMO case. But this specification leads to a too strong convection in REMO, due to the lack of the cooling of the SST by evaporation, which is present in ROM. These factors are reflected in the seasonality of the ITCZ precipitation: in DJF, REMO presents a better representation of the spatial distribution and intensity of the ITCZ precipitation (Fig. S2). ROM presents a double band in the ITCZ, a common trait in coupled models (Zhang et al., 2015). However, in JJA the ITCZ over South America is better represented by ROM, and its precipitation is closer to ERA5, especially over the Amazon.

As could be expected, strong differences between the coupled and

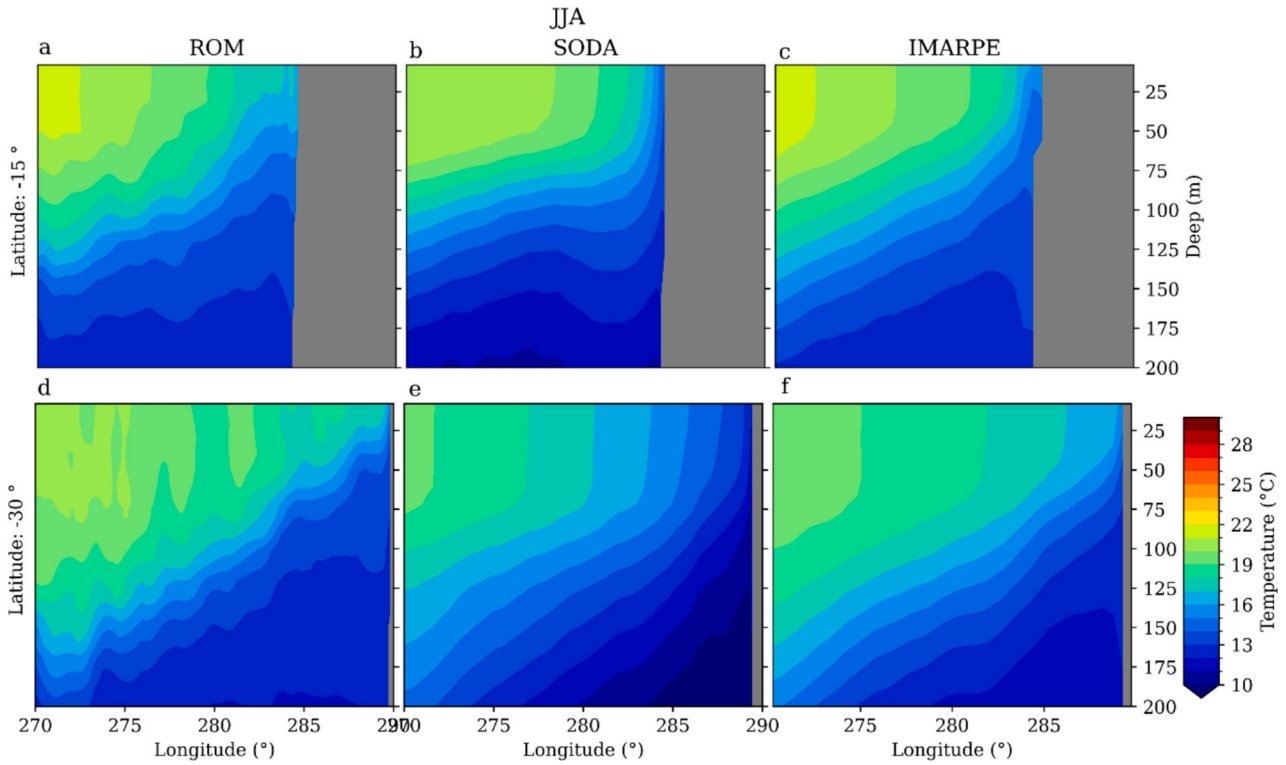


**Fig. 16.** Cross-shore temperature (°C) transect for DJF in 15°S (upper) and 30°S (lower) for ROM, SODA and IMARPE in JJA.

uncoupled simulations can be found in the lower levels of the atmosphere and in the precipitation. For instance, ROM improves the simulation of the position and intensity of the SPA as well as its seasonal migration (Fig. S5), which may be associated with the colder SST in the east and with warmer conditions in the west due to poleward advection of warmer air in the lower troposphere, which enhances the subtropical zonal SST gradient (Seager et al., 2003). Also, coupling provides a better representation of the seasonal cycle of sea level pressure in the Niño 1 + 2 and SPA regions. Moreover, ROM and REMO present similar values to the simulated interannual SLP variability for the period 1980–2017 in the two regions and for JJA and DJF, which is reflected in the Perkins score and the PDFs. However, the simulation of the interannual variability is better in REMO.

The coupling also improves the simulation of the temperature over land, with ROM showing a lower bias, as reflected in the AV. Some of these improvements are associated with a better representation of the monsoon system. Although the spatial distribution of the biases is similar in both models, the magnitude is lower in ROM. The DJF improvement in northeastern Brazil and Chaco plains could be related to a better simulation of the South American monsoon system (Vuille et al., 2012).

Over the ocean, DJF biases in ROM present a more complex pattern than in REMO, which presents only positive biases. The coupling leads to negative biases near the Pacific coasts, north of the equator and in the subtropics, with positive biases in the tropical interior oceans Over the ocean, the simulated T2m is strongly influenced by the SST. As in REMO the SST is prescribed (from ERA-Interim), the biases are stronger in ROM and reflect the modeled SST (Fig. S6). For instance, the cold biases off Chile coast and the warm bias along the Peruvian coast and the Niño 1 + 2 region, are likely related to the representation of the upwelling processes.

Coupling also influences the simulated precipitation over the continent, as is illustrated by the AV. Inland, outside the Andes, where convective precipitation is predominant, the biases show a similar spatial distribution, but their magnitude is different. The improvements that coupling brings to the simulation of the precipitation show a marked seasonality, which could be pointing to an improvement of the transport of humidity from the Atlantic ocean.

As shown above, even if the atmospheric model has an “ideal” oceanic forcing (ERA-Interim), a high resolution interactive SST could improve important features of the simulated atmospheric circulation, such as the SPA, the JJA ITCZ and the South American monsoon system. A better representation of atmospheric circulation leads to improved simulation of the surface air temperature and precipitation. However, our results show that SST biases (inherent in coupled models) can lead to a worsening of the simulation, understanding that the atmospheric circulation depends on the magnitude and spatial distribution of the SST, as in the case of the DJF ITCZ. In DJF, the spatial distribution of positive SST biases, covering the tropical Pacific, especially in the Niño 1 + 2 region, leads to the overestimation of precipitation in the ROM.

ROM allows us to simulate with high resolution the coupled ocean variability in the eastern Pacific, a region that is characterized by significant SST biases. The biases in the annual cycle are warmer than the observations during most of the year and although it reproduces well the interannual variability of the SST it is not able to simulate extraordinary events, underestimating the intensity as the strong El Niño (1983 and 1997). Both features seem to be related to a too thick thermocline that reduces the warming during El Niño events.

The ROM’s high oceanic resolution allows for a good simulation of the Humboldt upwelling. For instance, the coastal vertical structure is better resolved than in SODA and comparable with the observations, making ROM an useful tool for the study of the climate in this region, which harbors one of the most important ecosystems in the world.

When comparing the ROM and REMO simulations presented here one should keep in mind that for REMO we have used an “ideal” forcing both in the lateral and lower boundaries. Thus, the main results of this paper can be summarized as follows:

- Our regional coupled model shows the ability of improving important features of the climate in South America, especially in the western side of the Continent.
- Over the ocean, ROM improves the simulation of the South Pacific Anticyclone.
- The coupling improves the simulation of the precipitation in the regions affected by the transport of humidity from the ocean.
- The high ocean resolution allows for a good representation of the Humboldt Current upwelling system.
- ROM is a good tool for studying the climate of South America.

The results here give ground to the future use of ROM to gain a deeper insight into the South America by the end of twenty-first century.

## CRediT authorship contribution statement

**Jorge Ordoñez:** Writing – original draft, Methodology, Investigation, Data curation. **Jonathan Paredes:** Visualization, Formal analysis, Writing – original draft. **Rubén Vázquez:** Conceptualization, Investigation, Writing – original draft. **Alan Llacza:** Formal analysis, Methodology, Visualization. **Gerardo Jacome:** Methodology, Investigation. **Gustavo De la Cruz:** Validation, Investigation. **Jorge Llamocca:** Methodology, Investigation, Formal analysis. **Delia Acuña:** Project administration, Investigation, Formal analysis. **Dmitry V. Sein:** Supervision, Investigation, Data curation, Conceptualization. **Erick Álvarez:** Investigation, Methodology. **William Cabos:** Investigation, Methodology, Supervision, Writing – review & editing.

## Declaration of competing interest

The authors declare no conflicts of interest.

## Data availability statement

Please contact the authors.

## Acknowledgements

Simulations were done at the German Climate Computing Center (DKRZ), granted by its Scientific Steering Committee under project ID ba1207. J. Ordoñez, J. Paredes, A. Llacza, G. Jacome, G. De la Cruz, J. LLamocca and D. Acuña were supported by the Swiss Agency for Development and Cooperation and the Libelula Institute for Global Change. R. Vázquez and W. Cabos were supported by the Spanish Ministry of Science, Innovation and Universities, through grants (I+D+I PID2021-128656OB-I00). Dmitry Sein was supported by the Germany-Sino joint project (ACE, No. 2019YFE0125000 and 01LP2004A) and the scientific task N° FMWE-2024-0028 of MHESRF. The authors thank Dr. J. Sanabria for a careful reading of a preliminary version of the manuscript.

## Appendix A. Supplementary data

Supplementary data to this article can be found online at https://doi.org/10.1016/j.atmosres.2024.107447.

## References

Abatzoglou, J.T., Dobrowski, S.Z., Parks, S.A., Hegewisch, K.C., 2018. TerraClimate, a high-resolution global dataset of monthly climate and climatic water balance from 1958–2015. Sci. Data 5.

Ambrizzi, T., Reboita, M.S., da Rocha, R.P., Llopart, M., 2019. The state of the art and fundamental aspects of regional climate modeling in South America. Ann. N. Y. Acad. Sci. 1436, 98–120.

Ancapichún, S., Garcés-Vargas, J., 2015. Variability of the Southeast Pacific Subtropical Anticyclone and its impact on sea surface temperature off north-central Chile. Cienc. Mar. 41, 1–20.

Barrett, B.S., Hameed, S., 2017. Seasonal variability in precipitation in central and Southern Chile: modulation by the South Pacific high. J. Clim. 30 (1), 55–69. https://doi.org/10.1175/JCLI-D-16-0019.1.

Bielli, S., Barthe, C., Bousquet, O., Tulet, P., Pianezze, J., 2021. The effect of atmosphere-ocean coupling on the structure and intensity of tropical cyclone Bejisa in the Southwest Indian ocean. Atmosphere 12, 688.

Bruick, Z.S., 2019. Characteristics of Hailstorms and ENSO-Induced Extreme Storm Variability in Subtropical South America. Doctoral dissertation. Colorado State University. https://hdl.handle.net/10217/195364.

Cabos, W., Sein, D.V., Durán-Quesada, A., Liguori, G., Koldunov, N.V., Martínez-López, B., Alvarez, F., Sieck, K., Limareva, N., Pinto, J.G., 2019. Dynamical downscaling of historical climate over CORDEX Central America domain with a regionally coupled atmosphere–ocean model. Clim. Dyn. 52, 4305–4328.

Cabos, W., de la Vara, A., Álvarez-García, F.J., Sánchez, E., Sieck, K., Pérez, J.I., Limareva, N., Sein, D., 2020. Impact of ocean-atmosphere coupling on regional climate: the Iberian Peninsula case. Clim. Dyn. 54, 4441–4467. https://doi.org/10.1007/s00382-020-05238-x.

Cai, W., McPhaden, M.J., Grimm, A.M., et al., 2020. Climate impacts of the El Niño–Southern Oscillation on South America. Nat. Rev. Earth Environ. 1, 215–231. https://doi.org/10.1038/s43017-020-0040-3.

Carril, A.F., Menéndez, C.G., Remedio, A.R.C., Robledo, F., Sörensson, A., Tencer, B., Boulanger, J.P., de Castro, M., Jacob, D., Le Treut, H., Li, L.Z.X., Penalba, O., Pfeifer, S., Rusticucci, M., Salio, P., Samuelsson, P., Sanchez, E., Zaninelli, P., 2012. Performance of a multi-RCM ensemble for South Eastern South America. Clim. Dyn. 39, 2747–2768.

Carton, J.A., Chepurin, G.A., Chen, L., 2018. SODA3: a new ocean climate reanalysis. J. Clim. 31, 6967–6983. https://doi.org/10.1175/JCLI-D-18-0149.1.

Chen, T.-C., Weng, S.P., Schubert, S., 1999. Maintenance of austral summer upper-tropical circulation over tropical South America: the Bolivian high-Nordeste low system. J. Atmos. Sci. 56, 2081–2100.

de la Vara, A., Cabos, W., Sein, D.V., Teichmann, C., Jacob, D., 2021. Impact of air–sea coupling on the climate change signal over the Iberian Peninsula. Clim. Dyn. 57, 2325–2349. https://doi.org/10.1007/s00382-021-05812-x.

Domíngues, N., Grados, C., Vásquez, L., Gutiérrez, D., Chaigneau, A., 2017. Climatología termohalina frente a las costas del Perú. In: Periodo: 1981–2010. Informe IMARPE vol. 44 n°1, 2017. p. 5–13. https://hdl.handle.net/20.500.12958/3146.

Drumond, A., Marengo, J., Ambrizzi, T., Nieto, R., Moreira, L., Gimeno, L., 2014. The role of the Amazon Basin moisture in the atmospheric branch of the hydrological cycle: a Lagrangian analysis. Hydrol. Earth Syst. Sci. 18, 2577–2598. https://doi.org/10.5194/hess-18-2577-2014.

Espinoza, J.C., Garreaud, R., Poveda, G., Arias, P.A., Molina-Carpio, J., Masiokas, M., Viale, M., Scaff, L., 2020. Review Article. Hydroclimate of the Andes part I: Main Climatic Features. Front. Earth Sci. 8, 64. https://doi.org/10.3389/feart.2020.00064.

Falco, M., Carril, A.F., Menéndez, C.G., Zaninelli, P.G., Li, L.Z., 2019. Assessment of CORDEX simulations over South America: added value on seasonal climatology and resolution considerations. Clim. Dyn. 52, 4771.

Fouquart, Y., Bonnel, B., 1980. Computations of solar heating of the Earth's atmosphere: a new parameterization. Beitr. Phys. Atmos. 53, 35–62.

Funk, C., Peterson, P., Landsfeld, M., et al., 2015. The climate hazards infrared precipitation with stations—a new environmental record for monitoring extremes. Sci. Data 2, 150066. https://doi.org/10.1038/sdata.2015.66.

García-Reyes, M., Sydeman, W.J., Schoeman, D.S., Rykaczewski, R.R., Black, B.A., Smit, A.J., Bograd, S.J., 2015. Under pressure: climate change, upwelling, and eastern boundary upwelling ecosystems. Front. Mar. Sci. 2, 109. https://doi.org/10.3389/fmars.2015.00109.

Garreaud, R.D., Vuille, M., Compagnucci, R., Marengo, J., 2009. Present-day south American climate. Palaeogeogr. Palaeoclimatol. Palaeoecol. 281, 180–195.

Gent, P.R., Willebrand, J., McDougall, T., McWilliams, J.C., 1995. Parameterizing eddy-induced tracer transports in ocean circulation models. J. Phys. Oceanogr. 25, 463–474.

Giorgi, F., Torma, C., Coppola, E., et al., 2016. Enhanced summer convective rainfall at Alpine high elevations in response to climate warming. Nat. Geosci. 9, 584–589. https://doi.org/10.1038/ngeo2761.

Griffies, S.M., 1998. The Gent—McWilliams skew flux. J. Phys. Oceanogr. 28, 831–841.

Hagemann, S., Dumenil-Gates, L., 1998. A parameterization of the lateral water flow for the global scale. Clim. Dyn. 14, 17–31. https://doi.org/10.1007/s003820050205.

Hagemann, S., Dumenil-Gates, L., 2001. Validation of the hydrological v cycle of ECMWF and NCEP reanalysis using the MPI hydrological discharge model. J. Geophys. Res. 106 (D2), 1503–1510. https://doi.org/10.1029/2000JD900568.

Hersbach, H., Bell, B., Berrisford, P., et al., 2020. The ERA5 global reanalysis. Q. J. R. Meteorol. Soc. 146, 1999–2049.

Hibler, W.D., 1979. A dynamic thermodynamic sea ice model. J. Phys. Oceanogr. 9, 815–846.

Jacob, D., Podzun, R., 1997. "Sensitivity studies with the regional climate model REMO". Meteorology Atmospheric. Physics 63, 119¬129.

Jungclaus, J.H., Botzet, M., Haak, H., Keenlyside, N., Luo, J.-J., Latif, M., Marotzke, J., Mikolajewicz, U., Roeckner, E., 2006. Ocean circulation and tropical variability in the coupled model ECHAM5/MPI-OM. J. Clim. 19, 3952–3972.

Jungclaus, J.H., Fischer, N., Haak, H., Lohmann, K., Marotzke, J., Matei, D., Mikolajewicz, U., Notz, D., von Storch, J.S., 2013. Characteristics of the ocean simulations in MPIOM, the ocean component of the MPI-Earth system model. J. Adv. Model. Earth Syst. 5, 422–446. https://doi.org/10.1002/jame.20023.

Kämpf, J., Chapman, P., 2016. The Peruvian-Chilean Coastal Upwelling System. In: Upwelling Systems of the World. Springer, Cham. https://doi.org/10.1007/978-3-319-42524-5_5.

Kang, S.M., Xie, S.P., Shin, Y., Kim, H., Hwang, Y.T., Stuecker, M.F., Hawcroft, M., 2020. Walker circulation response to extratropical radiative forcing. Science advances 6 (47), eabd3021.

Lenters, J.D., Cook, K.H., 1997. On the Origin of the Bolivian High and Related Circulation Features of the south American climate. J. Atmos. Sci. 54 (5), 656–678.

Lewis, H.W., Castillo Sanchez, J.M., Graham, J., Saulter, A., Bornemann, J., Arnold, A., Fallmann, J., Harris, C., Pearson, D., Ramsdale, S., Martínez-de la Torre, A., Bricheno, L., Blyth, E., Bell, V.A., Davies, H., Marthews, T.R., O'Neill, C., Rumbold, H., O'Dea, E., Brereton, A., Guihou, K., Hines, A., Butenschon, M., Dadson, S.J., Palmer, T., Holt, J., Reynard, N., Best, M., Edwards, J., Siddorn, J., 2018. The UKC2 regional coupled environmental prediction system. Geosci. Model Dev. 11, 1–42.

Li, H., Kanamitsu, M., Hong, S.Y., 2012. California reanalysis downscaling at 10 km using an ocean-atmosphere coupled regional model system. J. Geophys. Res. 117, D12118. https://doi.org/10.1029/2011JD017372.

Llopart, M., Simões Reboita, M., Porfírio da Rocha, R., 2020. Assessment of multi-model climate projections of water resources over South America CORDEX domain. Clim. Dyn. 54, 99–116. https://doi.org/10.1007/s00382-019-04990-z.

Lohmann, U., Roeckner, E., 1996. Design and performance of a new cloud microphysics scheme developed for the ECHAM general circulation model. Clim. Dyn. 12, 557–572.

Marsland, S.J., Haak, H., Jungclaus, J.H., Latif, M., Roeske, F., 2003. The Max-Planck-Institute global ocean/sea ice model with orthogonal curvilinear coordinates. Ocean Model 5 (2), 91–126.

Mlawer, E.J., Taubman, S.J., Brown, P.D., Iaocono, M.J., Clough, S., 1997. Radiative transfer for inhomogeneous atmospheres: RRTM, validated correlated-k model for the longwave. J. Geophys. Res. 102, 16663–16682.

Nordeng, T.E., 1994. Extended Versions of the Convective Parameterization Scheme at ECMWF and Their Impact on the Mean and Transient Activity of the Model in the Tropics. ECMWF Technical Memorandum 206, 41.

Oyarzún, D., Brierley, C.M., 2019. The future of coastal upwelling in the Humboldt current from model projections. Clim. Dyn. 52, 599–615. https://doi.org/10.1007/s00382-018-4158-7.

Parras-Berrocal, I., Vazquez, R., Cabos, W., Sein, D., Mañanes, R., Perez-Sanz, J., Izquierdo, A., 2020. The climate change signal in the Mediterranean Sea in a regionally coupled ocean-atmosphere model. Ocean Sci 16, 743–765. https://doi.org/10.5194/os-16-743-2020.

Pauly, D., Christensen, V., 1995. Primary production required to sustain global fisheries. Nature 374, 255–257.

Penven, P., Echevin, V., Pasapera, J., Colas, F., Tam, J., 2005. Average circulation, seasonal cycle, and mesoscale dynamics of the Peru current system: a modeling approach. J. Geophys. Res. Oceans 110, C10021.

Perkins, S.E., Pitman, A.J., Holbrook, N.J., McAneney, J., 2007. Evaluation of the AR4 climate models' simulated daily maximum temperature, minimum temperature, and precipitation over Australia using probability density functions. J. Clim. 20 (17), 4356–4376.

Pezzi, L.P., Quadro, M.F.L., Souza, E.B., Miller, A.J., Rao, V.B., Rosa, E.B., Santini, M.F., Bender, A., Souza, R.B., Cabrera, M.J., Parise, C.K., Carvalho, J.T., Lima, L.S., de Quadros, M.R.L., Nehme, D.M., António, J.F., 2023. Oceanic SACZ produces an abnormally wet 2021/2022 rainy season in South America. Sci. Rep. 13, 1455. https://doi.org/10.1038/s41598-023-28803-w.

Rahn, D.A., Garreaud, R.D., 2014. A synoptic climatology of the near-surface wind along the west coast of South America. Int. J. Climatol. 34, 780–792. https://doi.org/10.1002/joc.3724.

Reboita, Michelle Simões, Porfírio, Rosmeri, da Rocha, Christie, de Souza, André, Baldoni, Thales Chile, Lopes, Pedro Lucas, da Silveira Silva, and Glauber Willian S. Ferreira., 2022. Future projections of extreme precipitation climate indices over South America based on CORDEX-CORE multimodel ensemble. Atmosphere 13 (9), 1463. https://doi.org/10.3390/atmos13091463.

Sánchez, E., Solman, S., Remedio, A.R.C., et al., 2015. Regional climate modelling in CLARIS-LPB: a concerted approach towards twentyfirst century projections of regional temperature and precipitation over South America. Clim. Dyn. 45, 2193.

Schemenauer, R.S., Fuenzalida, H., Cereceda, P., 1988. A Neglected Water Resource: the Camanchaca of South America. Bull. Am. Meteorol. Soc. 69 (2), 138–147. https://doi.org/10.1175/1520-0477(1988)069<0138:ANWRTC>2.0.CO;2.

Seager, R., Murtugudde, R., Naik, N., Clement, A., Gordon, N., Miller, J., 2003. Air–sea interaction and the seasonal cycle of the subtropical anticyclones. J. Clim. 16, 1948–1966.

Segura, H., Junquas, C., Carlo, J., Vuille, M., Jauregui, Y.R., Rabatel, A., Condom, T., Lebel, T., 2019. New insights into the rainfall variability in the tropical Andes on seasonal and interannual time scales. Clim. Dyn. https://doi.org/10.1007/s00382-018-4590-8.

Sein, D.V., Mikolajewicz, U., Gröger, M., Fast, I., Cabos, W., Pinto, J.G., Hagemann, S., Semmler, T., Izquierdo, A., Jacob, D., 2015. Regionally coupled atmosphere-ocean-sea ice-marine biogeochemistry model ROM: 1. Description and validation. J. Adv. Model. Earth Syst. 7, 268–304.

Sein, D.V., Gröger, M., Cabos, W., Alvarez-Garcia, F.J., Hagemann, S., Pinto, J.G., Izquierdo, I., De La Vara, A., Koldunov, N.V., Dvornikov, A.Y., Limareva, N., Aleekseva, E., Martinez-Lopez, B., Jacob, D., 2020. Regionally coupled atmosphere – ocean – marine biogeochemistry model ROM: 2.Studying the climate change signal in the North Atlantic and Europe. J. Adv. Model. Earth Syst. 0–3 p https://onlinelibrary.wiley.com/doi/abs/10.1029/2019MS001646.

Silvestri, G.E., Vera, C.S., 2003. Antarctic Oscillation signal on precipitation anomalies over southeastern South America. Geophys. Res. Lett. 30, 2115. https://doi.org/10.1029/2003GL018277, 21.

Silvestri, G., Vera, C., Jacob, D., Pfeifer, S., Teichmann, C., 2009. A high-resolution 43-year atmospheric hindcast for South America generated with the MPI regional model. Clim. Dyn. 32, 693–709.

Soares, P.M.M., Lima, D.C.A., Semedo, A., Cardoso, R.M., Cabos, W., Sein, D.V., 2019. Assessing the climate change impact on the North African offshore surface wind and coastal low-level jet using coupled and uncoupled regional climate simulations. Clim. Dyn. 1-22 https://doi.org/10.1007/s00382-018-4565-9.

Stark, J.D., Donlon, C.J., Martin, M.J., McCulloch, M.E., 2007. OSTIA: an operational, high resolution, real time, global sea surface temperature analysis system. In: OCEANS 2007—Europe, pp. 1–4. https://doi.org/10.1109/oceanse.2007.4302251.

Sulca, J., Takahashi, K., Espinoza, J.C., Vuille, M., Lavado-Casimiro, W., 2018. Impacts of different ENSO flavors and tropical Pacific convection variability (ITCZ, SPCZ) on austral summer rainfall in South America, with a focus on Peru. Int. J. Climatol. 38 (1), 420–435.

Takahashi, K., Mosquera, K., Reupo, J., 2014. El índice costero El Niño (ICEN): historia y actualización, boletín técnico "generación de modelos climáticos para el pronóstico de la ocurrencia del fenómeno El Niño". Inst. Geofís. Perú 1, 8–9.

Thompson, B., Sanchez, C., Heng, B.C.P., Kumar, R., Liu, J., Huang, X.-Y., Tkalich, P., 2021. Development of a MetUM (v 11.1) and NEMO (v 3.6) coupled operational forecast model for the maritime continent – part 1: evaluation of ocean forecasts. Geosci. Model Dev. 14, 1081–1100.

Tiedtke, M., 1989. A comprehensive mass flux scheme for cumulus parameterization in large-scale models. Mon. Weather Rev. 117, 1779–1800.

Valcke, S., 2013. The OASIS3 coupler: a European climate modelling community software. Geosci. Model Dev. 6, 373–388.

Vannière, B., Guilyardi, E., Toniazzo, T., et al., 2014. A systematic approach to identify the sources of tropical SST errors in coupled models using the adjustment of initialised experiments. Clim. Dyn. 43, 2261–2282. https://doi.org/10.1007/s00382-014-2051-6.

Vázquez, R., Parras-Berrocal, I., Cabos, W., Sein, D.V., Mañanes, R., Izquierdo, A., 2022. Assessment of the canary current upwelling system in a regionally coupled climate model. Clim. Dyn. 58, 69–85. https://doi.org/10.1007/s00382-021-05890-x.

Vázquez, R., Parras-Berrocal, I.M., Koseki, S., Cabos, W., Sein, D.V., Izquierdo, A., 2023. Seasonality of coastal upwelling trends in the Mauritania-Senegalese region under RCP8.5 climate change scenario. Sci. Total Environ. 898, 166391. ISSN 0048-9697. https://doi.org/10.1016/j.scitotenv.2023.166391.

Virji, H., 1981. A preliminary study of summertime tropospheric circulation patterns over South America estimated from cloud winds. Mon. Weather Rev. 109, 599–610.

Vuille, M., Burns, S.J., Taylor, B.L., Cruz, F.W., Bird, B.W., Abbott, M.B., Kanner, L.C., Cheng, H., Novello, V.F., 2012. A review of the South American monsoon history as recorded in stable isotopic proxies over the past two millennia. Clim. Past 8, 1309–1321. https://doi.org/10.5194/cp-8-1309-2012.

Weber, T., Cabos, W., Sein, D.V., et al., 2023. Benefits of simulating precipitation characteristics over Africa with a regionally-coupled atmosphere–ocean model. Clim. Dyn. 60, 1079–1102. https://doi.org/10.1007/s00382-022-06329-7.

Xie, S., Miyama, T., Wang, Y., Xu, H., de Szoeke, S.P., Small, R.J.O., Richards, K.J., Mochizuki, T., Awaji, T., 2007. A regional ocean–atmosphere model for eastern pacific climate: toward reducing tropical biases. J. Clim. 20 (8), 1504–1522. https://doi.org/10.1175/JCLI4080.1.

Xue, P., Malanotte-Rizzoli, P., Wei, J., Eltahir, E.A.B., 2020. Coupled ocean-atmosphere modeling over the maritime continent: a review. J. Geophys. Res. Oceans 125, 2019JC014978.

Zhang, X., Liu, H., Zhang, M., 2015. Double ITCZ in coupled ocean-atmosphere models: from CMIP3 to CMIP5. Geophys. Res. Lett. 42, 8651–8659. https://doi.org/10.1002/2015GL065973.

Zou, L.-W., Zhou, T.-J., 2011. Sensitivity of a regional ocean-atmosphere coupled model to convection parameterization over Western North Pacific. J. Geophys. Res. 116, D18106. https://doi.org/10.1029/2011jd015844.